Monitoring Common Skin Lesions using Thermography: A Preliminary Study

CRISTINA M. R. CARIDADE, LUÍS ROSEIRO
Department of Physics and Mathematics and Department of Mechanics,
Coimbra Institute of Engineering, Polytechnic of Coimbra,
Rua Pedro Nunes, Coimbra,
PORTUGAL

Abstract: - Infrared thermography is a non-invasive and non-radioactive diagnostic method based on the perception of the surface temperature of a body. Body temperature is an acceptable indicator of health conditions that can be used to monitor skin lesions. The development of a medical device for skin lesions can help clinical professionals evaluate patient registration, patient monitoring, and medical training. It can even be used as home care by the patient himself or as telemedicine. In this sense, this work arises, which aims to evaluate the accuracy about the detection and segmentation of common skin lesions obtained in a controlled environment, using a common thermographic camera and a thermographic camera for a smartphone. Some tests were carried out, with feet thermographic images of 2 volunteers (left foot and right foot) and an application was developed in MATLAB using image processing techniques that allow to automatically segment the region of interest and extract characteristics such as area, the minimum, maximum, average temperature and standard deviation of this region. The results show that the images acquired by a common thermographic camera are more accurate and reliable, but the control and monitoring are possible to be carried out with the thermographic smartphone camera, allowing many benefits since it is easy to access, low cost, and simple to use.

Key-Words: - Thermography, infrared thermography, infrared imaging, medical infrared, image processing, skin lesions, medical applications, monitoring, inflammatory injuries.

Received: April 7, 2024. Revised: October 19, 2024. Accepted: November 21, 2024. Published: December 31, 2024.

1 Introduction

Body temperature is an acceptable indicator of health conditions and has long been used to assess patient health, [1]. The skin, the largest organ in the human body, plays an essential role in this process, and most of the internal heat generated is spread to the surrounding environment by radiation. This can be recorded with infrared thermography imaging, [2]. Infrared thermography is a real-time, non-invasive, non-contact, and radiation-free imaging technology that provides information on variations in blood flow, often associated with injuries, resulting in changes in skin temperature, [3]. Recent studies have explored infrared thermographic cameras as a support for the diagnosis of skin lesions and inflammation, [4], [5], [6], [7]. However, this technology is expensive, not portable, and requires specialized knowledge, [8]. Considering the low cost and prevalence of smartphones, using a smartphone-based system has become an attractive option. There are many benefits to using a smartphone as a medical device, [9], [10], [11]. This device is easy to access, low cost, and simple to use. In addition, the medical device can help clinical professionals assess patient registration, patient monitoring, and medical training. It can even be used as home care by the patient himself or as telemedicine. However, the development of medical applications for smartphones using thermographic images is still an underdeveloped area. However the qualities of thermographic imaging cameras for use in smartphones in clinical practice have already been demonstrated, [12], [13], [14], [15].

Care of the bedridden patient at home involves caring for injuries to the skin and underlying tissues resulting from prolonged sitting or lying in one position. The frequent visits of elderly patients or patients with reduced mobility to the doctor or health professional to obtain the care they need is considered intrusive and expensive. The obligation of diabetic patients (types 1 and 2) to carry out a daily check of the feet, where it is necessary to analyze changes in temperature (hot or cold feet), color (normal, pale, red or blue), pain, swelling or any sign of infection. These and other cases can be solved by monitoring patients and exchanging medical information at a distance, using

telemedicine. The ability to store the patient's history and cross-reference the information and images captured digitally via telemedicine, brings many benefits to doctors and patients in defining ever faster and more accurate diagnoses.

In line with the development of an automatic system for the detection and monitoring of skin infections, based on thermographic images acquired by a camera associated with a smartphone, this work arises, which aims to evaluate the accuracy in relation to the automatic detection and segmentation of the region of interest of a skin infection obtained by this type of camera. For this, some tests were carried out in a controlled environment, where thermographic images were acquired using a common thermographic camera and a smartphone camera.

2 Methodology

A simple system was developed, consisting of two parts: thermographic image acquisition and an application for automatic segmentation and characteristic extraction (Figure 1). The thermographic image acquisition is composed of a smartphone, two thermographic cameras, a tripod, and a support to place the foot to be photographed (footrest).

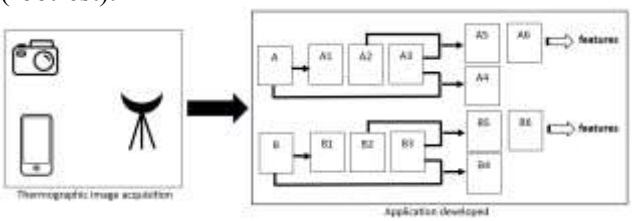

Fig. 1: Flowchart of the developed system

The thermographic cameras were placed on a tripod (Figure 2 bottom right), inside a platform (Figure 2 left) wrapped with black cloths in a dark laboratory, for the control and maintenance of light and ambient temperature.

Fig. 2: Thermographic image acquisition: platform (left); footrest (top right) and tripod (bottom right)

To acquire images of the foot in a stable way and always in the same position, a support (footrest) was created on a 3D printer (Figure 2 top right). The images were acquired at the feet of 2 volunteers using the *FLIR-T62101* camera (image A) and the *SEEK CompactPro USB-C* camera (image B) as shown in Figure 3. The volunteers followed an initial protocol to minimize the effects of factors that could influence the data. The volunteers took some precautions, such as: do not apply lotions or creams, do not expose the area to be photographed to the sun; do not perform physical activities that may affect body temperature and blood flow at the site examined for at least 4 hours before; do not smoke and avoid taking steroids, beta-blockers, vasoactive medications, opioids and contraceptive patches, among others.

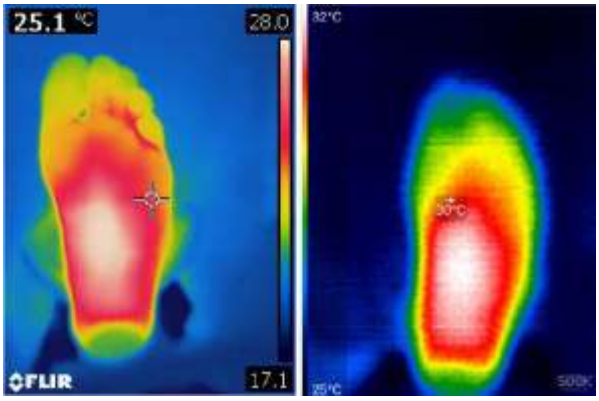

Fig. 3: Image of volunteer V1's left foot, taken by FLIR-T62101 camera (left) and SEEK CompactPro USB-C camera (right)

After the images were acquired (A and B), they were processed in an application developed in MATLAB [16] according to the flowchart shown in Figure 1 right. Initially, the color bars were automatically extracted from the original images (Figure 3) located on the right side (image A) and on the left side (image B), obtaining images A1 and B1 respectively (Figure 4 left). The resulting images are converted into grayscale images and pre-processing techniques are applied to improve their quality (images A2 and B2 in Figure 4 center), [17]. Thus, filters are applied to improve the contrast and lighting correction, and the histogram equalization is performed. Then, the images are converted to black and white images. Morphological operators are applied to these images, which allow the elimination of noise to be able to correctly identify the region of interest ROI (images A3 and B3 in Figure 4 right). Through this procedure, the ROI (region with possible infection) is automatically identified.

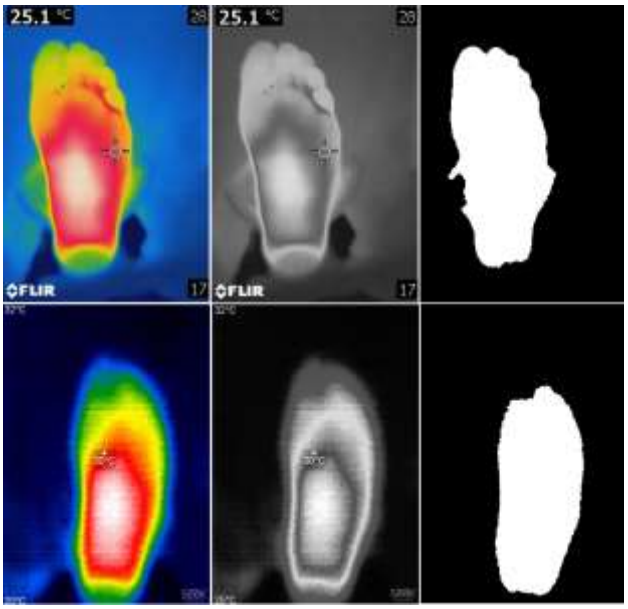

Fig. 4: Pre-processing of images A (top) and B (bottom): A1 and B1 original image without color bar (left); A2 and B2 grayscale image (center); A3 and B3 black and white image (right)

It is in this phase that, through character recognition, the maximum temperatures (Max) are read and recognized, which are found in the upper right corner of image A and in the upper left corner of image B (Figure 3). The procedure applied here consists of automatically identifying rectangular regions in the corners of the images (top, left, and right) and applying a character recognition algorithm. The same procedure is performed for the minimum temperatures (Min) found in the lower right corner A and lower left corner B. Then, applying images A3 and B3 as masks over image A and B respectively, it is possible to obtain only the ROI of the original images, that is, the segmented images A4 and B4 (Figure 5 left). In the same way, it is also possible to find the grayscale segmented images (by applying A3 and B3 to images A2 and B2, respectively), obtaining images A5 and B5 (Figure 5 right).

The next step consists of transforming the segmented image (A5 and B5) into an indexed image to the temperature bar (A6 and B6, respectively), i.e. transforming an image where each pixel represented by the intensity in grayscale is transformed into a temperature representation. Using Eq. (1) it is possible to calculate the temperature of each pixel of the image through its intensity (I) normalized between 0 and 1.

$$T = Min + (Max - Min) \times I \qquad (1)$$

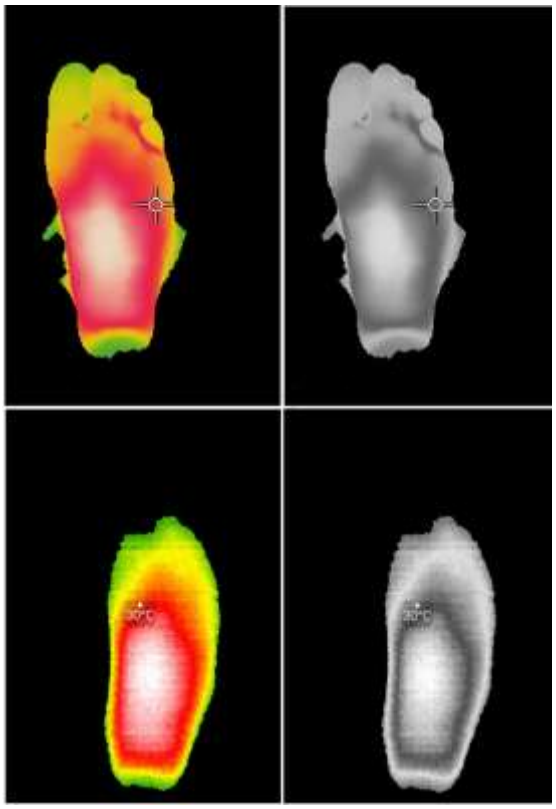

Fig. 5: Segmented images: starting from the original image (A4 and B4) and starting from the grayscale image (A5 and B5)

where Min is the minimum temperature and Max is the maximum temperature of an image identified through character recognition. For example, in image A2 (Figure 4 center), whose maximum temperature is $Max = 28$℃ and the minimum temperature is $Min = 17.1$℃, a pixel P with intensity $I = 0.5$, will have a temperature of $T = 17.1 + (28 - 17.1) \times 0.5 = 22.55$℃. This procedure is applied to all pixels of images A5 and B5, obtaining the indexed images (A6 and B6) with the corresponding temperature bar (Figure 6).

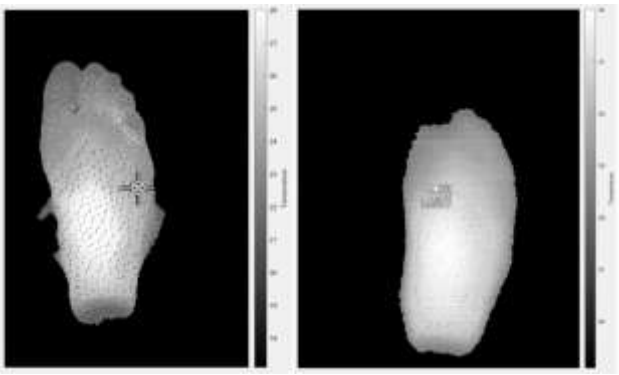

Fig. 6: Temperature images: indexed images (A6 and B6) obtained from the segmented images A5 and B5 (Figure 5)

Finally, the characteristics of this region, such as the amount of affected area (number of pixels), Max, Min, $Mean$ and standard deviation (Std), were evaluated to be used as indicators of the risk of infection. In this phase, the images obtained by the 2 cameras referring to the same foot and the same volunteer, are compared.

3 Results and Discussion

As an experimental study, 4 tests were performed T_i, $i = 1, \dots, 4$ on 2 volunteers (V_j, j=1,2), through the acquisition of thermography images of the left foot (LF_j, j=1,2) or right foot (RF_j, j=1,2) using the *FLIR-T62101* thermographic camera ($TC1$) and *SEEK CompactPro USB-C* ($TC2$). The regions of interest of the images were automatically obtained and their characteristics extracted. In the example shown in Figure 7, for volunteer V_1, it can be observed thermography image A1 acquired by camera $TC1$ (left) and thermography image B1 acquired by camera $TC2$ (right) of foot RF_1.

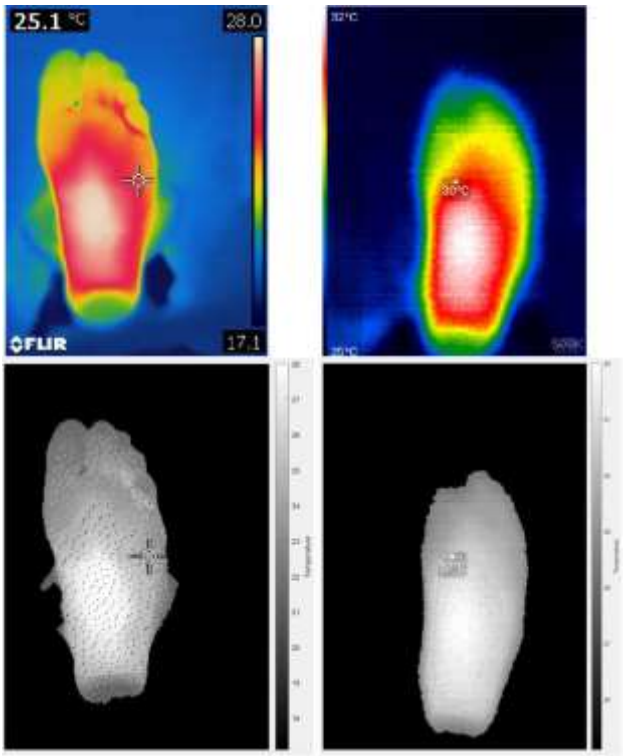

Fig. 7: Thermographic images A and B (top) and A6 and B6 (bottom) of the RF_1 foot of volunteer V_1 by camera $TC1$ (left) and $TC2$ (right)

The temperatures in image A vary between 17.1℃ and 28.0℃ and B between 25.0℃ and 32.0℃. A very significant difference both in the minimum temperature values ($Min = 25.0℃ - 17.1℃ = 7.9℃$) and in the maximum temperature values ($Max = 32.0℃ - 28.0℃ = 4℃$) as can be seen in the corresponding indexed images (Figure 7 bottom). This finding can also be confirmed in the histogram shown in Figure 8. This histogram represents the distribution of image pixels by temperature. There seems to be a shift between histograms of about 7 degrees. This is confirmed since the average temperature of A1 is 18.79℃ and B1 is 26.13℃ (Table 1), that is, a difference of 7.34℃. The standard deviation (Std) is 3.29 for A1 and 2.15 for B1, that is, less dispersion in the B1 image, therefore the temperatures of A1 vary more than those of B1.

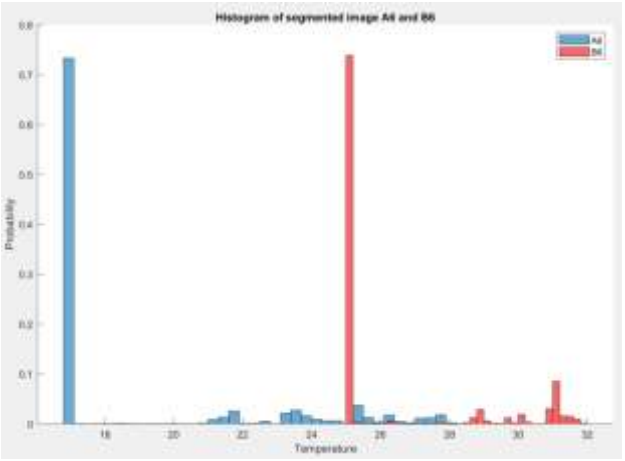

Fig. 8: Histogram of the A6 and B6 image

Regarding the ROI, the visual analysis established, it appears similar in the 2 images, although in A1 this region has a configuration more like a foot in relation to B1. This means that the accuracy of the first image is higher than that of the second image. On the other hand, image A1 has a dimension of 320 × 240 (=76800 pixels) and B1 of 640 × 480 (=307200), i.e. 4 times larger, and the ROI area of A1 is 19032 pixels and of B1 is 68055, i.e. 3.58 times bigger. Therefore, the ROI area of A1 is larger. Table 1 shows the characteristics obtained for all the tests carried out.

Table 1. Image ROI's characteristics

	T_1		T_2		T_3		T_4	
	$A1$	$B1$	$A1$	$B1$	$A1$	$B1$	$A1$	$B1$
Max	28.00	32.00	26.40	30.00	26.40	30.00	26.50	32.00
Min	17.10	25.10	17.70	25.00	17.60	25.00	18.60	26.00
$Mean$	18.79	26.13	19.18	25.53	18.94	25.52	19.59	27.19
Std	3.29	2.15	2.66	1.30	2.64	1.29	2.07	1.98
Px	19,032	68,055	20,263	48,979	18,901	48,844	18,819	91,587

Px means the number of pixels

Observing the general results, the Max and Min values are always higher for the 4 cases in image B1, in tests T_i, $i = 1, \dots, 4$. This means that the accuracy in terms of temperature in camera $TC2$ is lower than the accuracy in camera $TC1$, which was

already expected and possible to be verified visually. The difference in means is 7.34, 6.35, 6.58, 7.60 in the 4 cases (T_1 to T_4, respectively). It can also be concluded that the difference between the Max and Min value of the B1 images, in the $T_i,\ i = 1, \dots, 4$ tests is relatively smaller than the same difference for the A1 image of the same tests. Considering the notion of standard deviation, it makes sense that the values of this for type B images are lower than the standard deviation values for type A images.

4 Conclusion

The work presented, had as main objective to develop an application in MATLAB that analyses and compares thermographic images obtained by thermographic cameras of different cost/quality. To evaluate the applicability of using the low-cost camera for the control and monitoring of skin lesions, since it is easy to access, low cost, and simple to use. Its use by clinical professionals is extremely useful and important to evaluate patient registration, patient monitoring, and medical training in hospitals, health care centers, or in-home care.

The acquisition of images by the two cameras followed a control protocol both in the system developed for the acquisition of thermographic images and in the procedures followed by the volunteers.

The developed application allows comparing the thermographic images acquired by the two cameras. Automatically, the images are read by the application, and using image processing techniques and methods, the region of interest is segmented and characteristics that define these regions are extracted, thus allowing a comparative analysis of both the size of the segmented region (number of pixels) and the temperatures involved in that region, such as the minimum, maximum, average and standard deviation.

To evaluate the possibility of using the low-cost camera as a means of acquiring thermographic images for the control and monitoring of skin lesions, 4 simulations were performed. Analysis of the results indicates that camera A exhibits lower temperatures compared to camera B. For example, in simulations T_1, T_2, T_3, T_4, the average temperature for camera B is always higher than that for camera A, which may indicate greater thermal sensitivity of B. This difference can be attributed to the calibration and thermal response of the camera, which, despite being less accurate, shows a greater variation in measurements. Camera A has a larger standard deviation than camera B in all tests. Greater variability observed in camera A suggests that it may be capturing a wider range of thermal data, which could be advantageous in certain contexts, but could also pose a challenge in terms of measurement accuracy and consistency. Camera B presents a greater number of pixels in several simulations, which implies that the thermal region analyzed is more extensive or covered with greater data density (greater coverage of ROI). Camera A is superior in terms of accuracy and consistency in thermal measurements and is therefore more suitable for detecting small thermal variations.

Thus, camera B may be advantageous for monitoring larger areas and may be a good option for general monitoring of skin conditions. However, camera A, despite having a smaller pixel area, offers greater accuracy and consistency in thermal measurements, making it more reliable for detailed diagnoses and for identifying small thermal variations in skin lesions. The use of both cameras can be complementary: camera B can be used for an overview and monitoring of large areas, while camera A provides a more detailed and precise analysis, especially for more critical diagnoses. The choice between cameras should therefore depend on the specific monitoring or diagnostic objective, considering the balance between coverage of the area of interest and the accuracy of thermal measurements.

As future work, it is intended to test the application developed on a wide variety of patients with different types of skin lesions, using both cameras and adapting the image acquisition protocol to the specific conditions of hospital environments or health care centers. In this context, it will be necessary to adjust the approach to obtaining thermographic images, considering the particularities of these environments, such as the available infrastructure and the characteristics of the patients. This process will make it possible to validate the results obtained in this study and make the necessary adaptations to the characteristics to be collected.

Acknowledgement:
The author C. Caridade teaches and does research at Coimbra Institute of Engineering, Polytechnic of Coimbra, Coimbra, and CICGE, DGAOT, FCUP, Vila Nova de Gaia, Portugal, and Research Centre for Natural Resources Environment and Society (CERNAS), Polytechnic Institute of Coimbra, Portugal and Research Group on Sustainability

Cities and Urban Intelligence (SUScita), Polytechnic Institute of Coimbra, Coimbra, Portugal; L. Roseiro teaches and does research at Coimbra Institute of Engineering, Polytechnic of Coimbra, Coimbra and Applied Biomechanics Laboratory (LBA) of Coimbra Institute of Engineering, Polytechnic of Coimbra.

Declaration of Generative AI and AI-assisted Technologies in the Writing Process

The authors wrote, reviewed and edited the content as needed and they have not utilized artificial intelligence (AI) tools. The authors take full responsibility for the content of the publication.

References:

[1] Lahari, B.B., Bagavathiappan, S., Jaykumar, T., Philip, J.: Medical applications of infrared thermography: A review. *Infrared Physics & Technology,* Vol. 55, No. 4, pp. 221-235 (2012). https://doi.org/10.1016/j.infrared.2012.03.007

[2] Vardasca, R., Magalhaes, C., Silva, P., Abreu, P., Mendes, J., Restivo, M.T.: Biomedical musculoskeletal applications of infraredthermal imaging on arm and forearm: A systematic review. *Journal of thermal Biology,* Vol. 82, pp. 164-177 (2019). https://doi.org/10.1016/j.jtherbio.2019.04.008.

[3] Faerber, J., Ngoie, J.: Integration of a mobile application using medical infrared imaging to improve the effectiveness of physiotherapy treatments. 2019. *CMBES Proceedings (2019),* Ottawa, Ontario.

[4] Derruau, S., Bogard, F., Exartier-Menard, G., Mauprivez, C., Polidori, G.: Medical infrared thermography in odontogenic facial cellulitis as a clinical decision support tool. A technical note. *Diagnostics,* Vol. 11. No. 11, 2045 (2021). https://doi.org/10.3390/diagnostics11112045.

[5] Ramirez-GarciaLuna, J.L., Bartlett, R., Arriaga-Caballero, J.E., Fraser, R.D., Saiko, G.: Infrared thermography in wound care, surgery, and sports medicine: a review. *Frontiers in physiology,* Vol. 13, No. 210 (2022). https://doi.org/10.3389/fphys.2022.838528.

[6] Schiavon, G., Capone, G., Frize, M., Zaffagnini, S., Candrian, C., Filardo, G.: Infrared thermography for the evaluation of inflammatory and degenerative joint diseases: a systematic review. *Cartilage,* Vol. 13, No. 2_suppl, 1790S-1801S (2021). https://doi.org/10.1177/194760352110638

[7] Barson, C., Saatchi, R., Godbole, P., Ramlakhan, S.: Infrared thermal imaging to detect inflammatory intra-abdominal pathology in infants. W*SEAS Transactions on Biology and Biomedicine,* Vol. 17, pp. 82-98, (2020). https://doi.org/10.37394/23208.2020.17.16.

[8] Niri, R., Lucas, Y., Treuillet, S., Douzi, H.: Smartphone-based thermal imaging system for diabetic foot ulcer assessment. In *Journées d'Etude sur la TéléSanté Sorbonne Universités,* May 2019, Paris, France. ffhal-02161044f.

[9] Agu, E., Pedersen, P., Strong, D., Tulu, B., He, Q., Wang, L., Li, Y.: The smartphone as a medical device: Assessing enablers, benefits and challenges. I*n 2013 IEEE International Workshop of Internet-of-Things Networking and Control (IoT-NC) IEEE,* pp. 48-52 (2013). https://doi.org/10.1109/IoT-NC.2013.6694053.

[10] Fleming, G.A., Petrie, J.R., Bergenstal, R.M., Holl, R. W., Peters, A.L., Heinemann, L.: Diabetes digital app technology: benefits, challenges, and recommendations. A consensus report by the European Association for the Study of Diabetes (EASD) and the American Diabetes Association (ADA) Diabetes Technology Working Group. Diabetes care, Vol. 43, No. 1, pp. 250-260 (2020). https://doi.org/10.2337/dci19-0062.

[11] Chug, M.K., Brisbois, E.J.: Smartphone compatible nitric oxide releasing insert to prevent catheter-associated infections. *Journal of Controlled Release,* Vol. 349, pp. 227-240 (2022). https://doi.org/10.1016/j.jconrel.2022.06.043.

[12] Van Doremalen, R.F.M., Van Netten, J.J., Van Baal, J.G., Vollenbroek-Hutten, M.M.R., van der Heijden, F.: Validation of low-cost smartphone-based thermal camera for diabetic foot assessment. *Diabetes research and clinical practice,* Vol. 149, pp. 132-139 (2019). https://doi.org/10.1016/j.diabres.2019.01.032

[13] Caridade, C.M.R., Roseiro, L.: Automatic segmentation of skin regions in thermographic images: an experimental study. *WSEAS Transactions on Signal Processing,* Vol. 17, pp. 57-64, (2021). https://doi.org/10.37394/232014.2021.17.7.

[14] Wilson, A.C., Jungbauer, W.N., Hussain, F.T., Lindgren, B.R., Lassig, A.A.D.:

Characterization of baseline temperature characteristics using thermography in the clinical setting. *Journal of Surgical Research,* Vol. 272, pp. 26-36 (2022). https://doi.org/10.1016/j.jss.2021.11.006.

[15] Castonguay, T., Dover, G.: Infrared Thermography—A Novel Tool for Monitoring Fracture Healing: A Critically Appraised Topic With Evidence-Based Recommendations for Clinical Practice. *Journal of Sport Rehabilitation,* 1(aop), pp. 1-6 (2023). https://doi.org/10.1123/jsr.2022-0390.

[16] The MathWorks Inc. (2022). MATLAB version: 9.13.0 (R2022b), Natick, Massachusetts: The MathWorks Inc., [Online]. https://www.mathworks.com (Accessed Date: November 8, 2024).

[17] Gonzalez, R.C., Woods, R.E.: *Digital Image Processing.* 4th Edition. Pearson (2018). ISBN: 978-1-292-22304-9.

Contribution of Individual Authors to the Creation of a Scientific Article (Ghostwriting Policy)

The authors equally contributed in the present research, at all stages from the formulation of the problem to the final findings and solution.

Sources of Funding for Research Presented in a Scientific Article or Scientific Article Itself

No funding was received for conducting this study.

Conflict of Interest

The authors have no conflicts of interest to declare.